Examination of Relationships between Clear-Sky Longwave Radiation and Aspects of the Atmospheric Hydrological Cycle in Climate Models, Reanalyses, and Observations

RICHARD P. ALLAN

Environmental Systems Science Centre, University of Reading, Reading, United Kingdom

(Manuscript received 5 May 2008, in final form 8 December 2008)

ABSTRACT

Relationships between clear-sky longwave radiation and aspects of the atmospheric hydrological cycle are quantified in models, reanalyses, and observations over the period 1980–2000. The robust sensitivity of clear-sky surface net longwave radiation (SNLc) to column-integrated water vapor (CWV) of 1–1.5 W m^{-2} mm^{-1} combined with the positive relationship between CWV and surface temperature (T_s) explains substantial increases in clear-sky longwave radiative cooling of the atmosphere (Q_{LWc}) to the surface over the period. Clear-sky outgoing longwave radiation (OLRc) is highly sensitive to changes in aerosol and greenhouse gas concentrations in addition to temperature and humidity. Over tropical ocean regions of mean descent, Q_{LWc} increases with T_s at ~3.5–5.5 W m^{-2} K^{-1} for reanalyses, estimates derived from satellite data, and models without volcanic forcing included. Increased Q_{LWc} with warming across the tropical oceans helps to explain model ensemble mean increases in precipitation of 0.1–0.15 mm day^{-1} K^{-1}, which are primarily determined by ascent regions where precipitation increases at the rate expected from the Clausius–Clapeyron equation. The implications for future projections in the atmospheric hydrological cycle are discussed.

1. Introduction

Projected changes in the global water cycle are expected to exert an adverse effect on agriculture, water resources, human health, and infrastructure (Adger et al. 2007). Monitoring and understanding the present-day changes in the atmospheric hydrological cycle, including radiative feedbacks, are crucial in evaluating and improving model predictions of future climate change and its effect on society.

One of the driving influences for radiative feedbacks and changes in the hydrological cycle is the robust positive relationship between atmospheric water vapor and surface temperature due to the Clausius–Clapeyron equation (e.g., Allen and Ingram 2002; Trenberth et al. 2003; Soden et al. 2005; Wentz et al. 2007). Model predictions of future changes in precipitation depend crucially on climate feedbacks that determine how much the planet will warm in response to a radiative forcing from increased concentrations of greenhouse gases. This warming influences the hydrological cycle in two ways. First, increased atmospheric moisture, in response to the warming, allows enhanced convective rainfall (e.g., Trenberth et al. 2003). Second, the atmospheric radiative cooling enhances with increased warming (e.g., Allen and Ingram 2002), and this drives increases in precipitation through reduced atmospheric stability (the latent heating must rise to balance the stronger radiative cooling). The expected increases in precipitation through this second effect are smaller than the rises in convective precipitation through enhanced moisture convergence; to compensate, precipitation must diminish away from the convective regimes.

The tendency for increased precipitation for convective regimes and reduced precipitation for nonconvective regimes has been identified in modeling and observational studies (Allan and Soden 2007; Chou et al. 2007; Emori and Brown 2005; Neelin et al. 2006; Seager et al. 2007). However, there is evidence that models are underestimating the response of the hydrological cycle both for precipitation (Allan and Soden 2007; Zhang et al. 2007; Wentz et al. 2007) and evaporation (Yu and Weller 2007; Wentz et al. 2007; Yu 2007). It is important to ascertain whether this discrepancy relates to inadequacies of the observing system or to unresolved decadal variability by the models.

Corresponding author address: Richard Allan, Environmental Systems Science Centre, Harry Pitt Building, University of Reading, Reading, Berkshire RG6 6AL, United Kingdom.
E-mail: rpa@mail.nerc-essc.ac.uk

DOI: 10.1175/2008JCLI2616.1

Since changes in cloud and aerosol remain under scrutiny (Wielicki et al. 2002; Trenberth 2002; Mishchenko et al. 2007; Wild et al. 2005), it is first important to establish that models can reproduce the most well-understood coupling between surface temperature and precipitation, relating to changes in moisture and clear-sky radiation. Thus, the present study seeks to quantify relationships between surface temperature, moisture, clear-sky radiation, and precipitation using current climate model simulations, reanalyses, and observationally derived quantities over the period 1980–2000. While relating interannual relationships to longer-time-scale changes is problematic, the aim is to assess the processes that are key to clear-sky radiative feedbacks (e.g., Shell et al. 2008) and changes in the atmospheric hydrological cycle by quantifying the relationships between these important aspects of the climate system.

2. Method, data, and models

Monthly-mean data, from the observations, reanalyses, and models described in this section, were bilinearly interpolated to a common 2.5° × 2.5° grid. Area-weighted mean time series were calculated and deseasonalized. Linear least squares fits were applied to quantify significant relationships at the 95% confidence level allowing for autocorrelation (Yang and Tung 1998), and calculations were performed on varying geographical domains and partitioned between ocean and land grid points. Also, the ascending and descending portions of the tropical circulation were diagnosed for each month using 500-hPa vertical motion fields (e.g., Allan 2006). The 20-yr period 1980–2000 is considered to maximize overlap between observations, reanalyses, and model experiments and also because negative trends in clear-sky longwave radiation from satellite since 2000 are questionable (e.g., Allan 2007).

a. Observations

Observations of column-integrated water vapor (CWV) over the ice-free oceans were provided by the Scanning Multichannel Microwave Radiometer (SMMR; Wentz and Francis 1992) for 1979–84 and the Special Sensor Microwave Imager (SSM/I, version 6; Wentz et al. 2007) for 1987–2000. Surface temperatures (T_s) over the ice-free oceans were taken from the Hadley Centre Global Sea Ice and Sea Surface Temperature (HadISST) dataset (Rayner et al. 2003). The surface net longwave radiation for clear-skies (SNLc) was estimated over the ocean using the semiempirical formula of Prata (1996) with input from SSM/I CWV, the HadISST T_s, and a surface minus near-surface temperature difference climatology (Allan 2006). SNLc is calculated as the downward minus upward flux and therefore is predominantly negative.

Monthly-mean clear-sky outgoing longwave radiation (OLRc) data were taken from the Earth Radiation Budget Satellite (ERBS) for the period 1985–89, the Scanner for Radiation Budget (ScaRaB) for 1994/95, and the Clouds and the Earth's Radiant Energy System (CERES) on the Tropical Rainfall Measuring Mission (TRMM) satellite for 1998 (version ES4_TRMM-PFM_EDITION2_015013). These data, described in Wielicki et al. (2002), were considered only for the tropics (30°S–30°N). Clear-sky net longwave radiative cooling of the atmosphere (Q_{LWc}) is calculated as the sum of OLRc and SNLc. Although thermal satellite data samples systematically drier profiles than the models, leading to a well-documented bias (e.g., Sohn and Bennartz 2008), changes in mean OLRc are not strongly influenced by this effect (Allan et al. 2003) and so are included in the comparison. Nevertheless, the clear-sky satellite data are also subject to cloud contamination and calibration limitations.

Precipitation (P) over the tropical oceans was supplied by Wentz et al. (2007) over the period July 1987–December 1999, excluding the month of December 1987 because of missing data. Global estimates of precipitation were also taken from the Global Precipitation Climatology Project (GPCP; Adler et al. 2008) and the Climate Prediction Center Merged Analysis of Precipitation (CMAP; Xie and Arkin 1998) enhanced product (V703) for 1980–2000.

b. Reanalyses

Monthly-mean data were extracted from the National Centers for Environmental Prediction–National Center for Atmospheric Research reanalysis 1 (NCEP; Kalnay et al. 1996) and from the 40-yr European Centre for Medium-Range Weather Forecasts (ECMWF) Re-Analysis (ERA-40; Uppala et al. 2005). The 24-h forecasts from ERA-40 are used since these provide improved simulations of water vapor and clear-sky longwave radiation variability over oceans compared with the standard products (Uppala et al. 2005; Allan 2007). Precipitation was not considered, because of spurious variability (Uppala et al. 2005), but 500-hPa vertical motion fields (ω) were exploited to subsample ascending and descending branches of the tropical circulation for use with the observational data.

Also considered is release 2.5 of the National Aeronautics and Space Administration (NASA) Surface Radiation Budget (SRB) longwave product (http://eosweb.larc.nasa.gov/PRODOCS/srb/readme/readme_srb_rel2.5_lw_daily.txt). This is similar to the SRB product described in Allan (2006) but the updated Goddard Earth

TABLE 1. Description of model data. NV = no volcanic eruptions, V = volcanic eruptions, bold signifies ensemble member. Model data were taken from the WCRP CMIP3 database (Meehl et al. 2007).

	Model	Resolution	AMIP3	CMIP3	Reference
1	CCCMA.CGCM3.1	T47 L31		**NV**	Kim et al. (2002)
2	CCCMA.CGCM3.1.T63	T63 L31		**NV**	Kim et al. (2002)
3	CNRM.CM3	T63 L45	NV	**NV**	Salas-Mélia et al. (2005)
4	CSIRO.MK3.0	T63 L18		NV	Gordon et al. (2002)
5	GFDL.CM2.0	2.5° × 2° L24		**V**	Delworth et al. (2006)
6	GFDL.CM2.1	2.5° × 2° L24		**V**	Delworth et al. (2006)
7	GISS.MODEL.E.R	5° × 4° L13	V(3)	**V**	Schmidt et al. (2006)
8	INMCM3.0	5° × 4° L21	**NV**	**V**	Volodin and Diansky (2004)
9	IPSL.CM4	2.5° × 3.75° L19	**NV**	**NV**	Marti et al. (2005)
10	MIROC3.2.HIRES	T106 L56	**NV**	**V**	Hasumi and Emori (2004)
11	MIROC3.2.MEDRES	T42 L20	**NV**	**V**	Hasumi and Emori (2004)
12	MPI.ECHAM5	T63 L31	NV	**NV**	Jungclaus et al. (2006)
13	MRI.CGCM2.3.2A	T42 L30	**NV**	**NV**	Yukimoto and Noda (2002)
14	NCAR.CCSM3.0	T85 L26	NV	V	Collins et al. (2006)
15	NCAR.PCM1	T42 L30	NV	V/NV	Washington et al. (2000)
16	UKMO.HADCM3	3.75° × 2.5° L19		NV	Gordon et al. (2000)
17	UKMO.HADGEM1	1.875° × 1.25° L38	NV	V/NV	Johns et al. (2006)

Observing System (GEOS)-4 reanalysis product is used instead of GEOS-1 and the data cover the period 1983–2005.

c. Model data

Monthly-mean model data, for the period 1980–2000, was extracted from the World Climate Research Programme (WCRP) model archive at the Program for Climate Model Diagnosis and Intercomparison (PCMDI) archive (additional information is available online at www-pcmdi.llnl.gov; Meehl et al. 2007). Two families of experiments were considered: atmosphere models forced with observed sea surface temperature [Atmospheric Model Intercomparison Project (AMIP3)] and fully coupled atmosphere–ocean models [Coupled Model Intercomparison Project (CMIP3)] to which best estimates of radiative forcing were applied [climate of the twentieth-century experiments (20C3M)]. These experiments were further partitioned depending upon whether volcanic forcing was applied (see Table 1). Where surface longwave emission was not provided, this was calculated as σT_s^4. Clear-sky surface downwelling longwave radiation from the National Center for Atmospheric Research (NCAR) Parallel Climate Model (PCM1) model was found to be spurious and corrected fields were supplied. Least squares linear fits between variables were calculated separately for each model ensemble member and additionally for intermodel ensemble means; only data from selected models were used, depending upon the availability of all fields considered in the present study. These models are highlighted in bold in Table 1; the model experiments in which volcanic forcings were included (V) and were not included (NV) are also denoted. The run1 ensemble member from each model was used in the intermodel ensemble except for the Canadian Centre for Climate Modelling and Analysis Coupled General Circulation Model, version 3 (CCCMA CGCM3), and Goddard Institute for Space Studies Model E-R (GISS-ER) models in which the run2 ensemble member was used.

3. Global comparison

Multiannual global-mean quantities for the reanalyses products and model ensemble means are documented in Table 2. The model ensemble means underestimate CWV by 5%–8% and OLRc by 1–3 W m^{-2} compared to ERA-40 (the volcanically forced CMIP3 ensemble has the largest discrepancy), consistent with a low-level dry bias and a mid–high-tropospheric cold and moist bias in the models (John and Soden 2007). The low-level dry bias explains overly negative SNLc, although the regional distribution of the differences is more complex (Bodas-Salcedo et al. 2008). There is also evidence that inaccuracies in radiation codes contribute to an underestimate in SNLc, in particular for cold, dry climates for older models (Wild 2008). The discrepancy in SNLc and OLRc explains a model underestimate in Q_{LWc} of 8 W m^{-2} compared to ERA-40. The Meteorological Research Institute Coupled General Circulation Model version 2 (MRI CGCM2) CMIP3 model simulated the lowest OLRc (257 W m^{-2}) and CWV (21 mm), consistent with a substantial cold bias (−2 K) and lower-tropospheric dry bias (−10%) compared with independent satellite data (John and Soden 2007), and also simulates one of the lowest mean Q_{LWc} (169 W m^{-2}) and

TABLE 2. Global–annual-mean clear-sky radiation, water vapor, and precipitation for reanalyses and climate model ensemble mean, 1980–2000.

Dataset	T_s (K)	CWV (mm)	SNLc (W m^{-2})	Q_{LWc} (W m^{-2})	OLRc (W m^{-2})	P (mm day^{-1})
ERA-40–GPCP	287.58	24.50	−82.16	183.03	265.20	2.61
NCEP–CMAP	287.79	23.90	−85.88	182.76	268.64	2.67
SRB	287.72	—	−87.49	180.69	268.18	—
AMIP ensemble	288.07	23.30	−89.24	174.48	263.73	2.77
CMIP ensemble nonvolcanic	287.33	23.22	−87.30	176.34	263.64	2.80
CMIP ensemble volcanic	287.60	22.45	−87.23	174.77	262.00	2.84

P (2.57 mm day^{-1}). The multimodel ensemble means for P are 4%–9% larger than GPCP–CMAP estimates.

Individual models with higher Q_{LWc} tend to simulate larger P (Fig. 1a). Based on a linear fit to the models, differences in Q_{LWc} explain over 40% of the variance in P, suggesting that clear-sky longwave radiative cooling is a significant factor in explaining model precipitation. This importance is more apparent when considering interannual variability: Fig. 1b shows annual-mean anomalies in P and Q_{LWc} for the AMIP3 and CMIP3 experiments of the Hadley Centre Global Environmental Model version 1 (HadGEM1) model. Years with positive Q_{LWc} anomalies tend to coincide with higher precipitation; the explained variance is 70%. This highlights the contribution of the clear-sky longwave cooling of the atmosphere toward balancing latent heating via precipitation in models, both in a mean sense and also for variability, and forms the motivation for assessing the links between longwave radiative cooling and the hydrological cycle in models, reanalyses, and observations. Nevertheless, it should be noted that differences in shortwave atmospheric radiation budgets, poorly simulated in climate models (Wild 2008), may also contribute to errors in the hydrological cycle, both in terms of the mean state and variability. For example, underestimates in model ensemble mean Q_{LWc} are of the wrong sign to explain an apparent overestimate in P compared to GPCP and CMAP. While the precise accuracy of GPCP and CMAP precipitation totals are questionable, it is likely that model underestimation of shortwave atmospheric absorption by aerosol and water vapor (Wild 2008) and uncertainty in cloud longwave radiative forcing (Lambert and Webb 2008; Bodas-Salcedo et al. 2008) and near-surface conditions (Richter and Xie 2008) may contribute to errors in model precipitation and its response to warming.

Deseasonalized global monthly-mean anomalies are shown for the reanalyses, GPCP precipitation, and the AMIP3 models (Fig. 2), with the shaded area denoting the ensemble mean ± 1 standard deviation. Least squares linear fits between variables for the models, reanalyses, and the GPCP–CMAP precipitation data are displayed in Fig. 3. Regressions are applied separately to each model ensemble member and also to the multimodel ensemble mean (horizontal broken lines) for nonvolcanic AMIP3 models (black), nonvolcanic CMIP3 models (blue), and volcanic CMIP3 models (green); the ensemble members and the model number are detailed in Table 1. Vertical lines signify ± 1 standard error in the linear fit for each model ensemble member; boxes

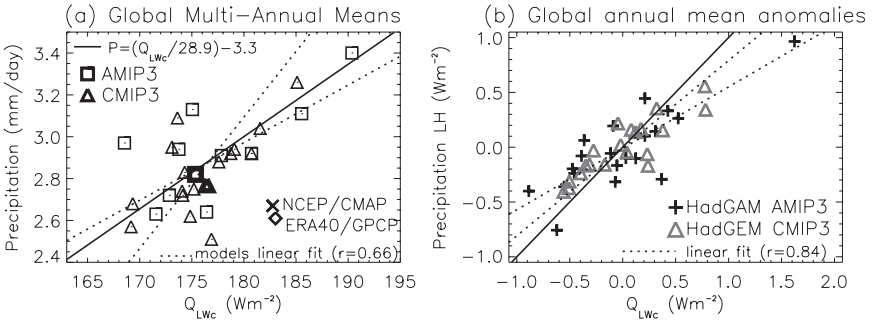

FIG. 1. Relationship between precipitation and clear-sky longwave radiative cooling of the atmosphere for (a) models and reanalyses multiannual means and (b) annual-mean anomalies over the period 1980–2000 for the HadGEM AMIP3 and CMIP3 experiments. Also shown are the range in linear fits to the AMIP3/CMIP3 models (dotted lines) and the $dP/dQ_{\mathrm{LWc}} = 1$ line where P is converted to units of W m^{-2} (solid lines).

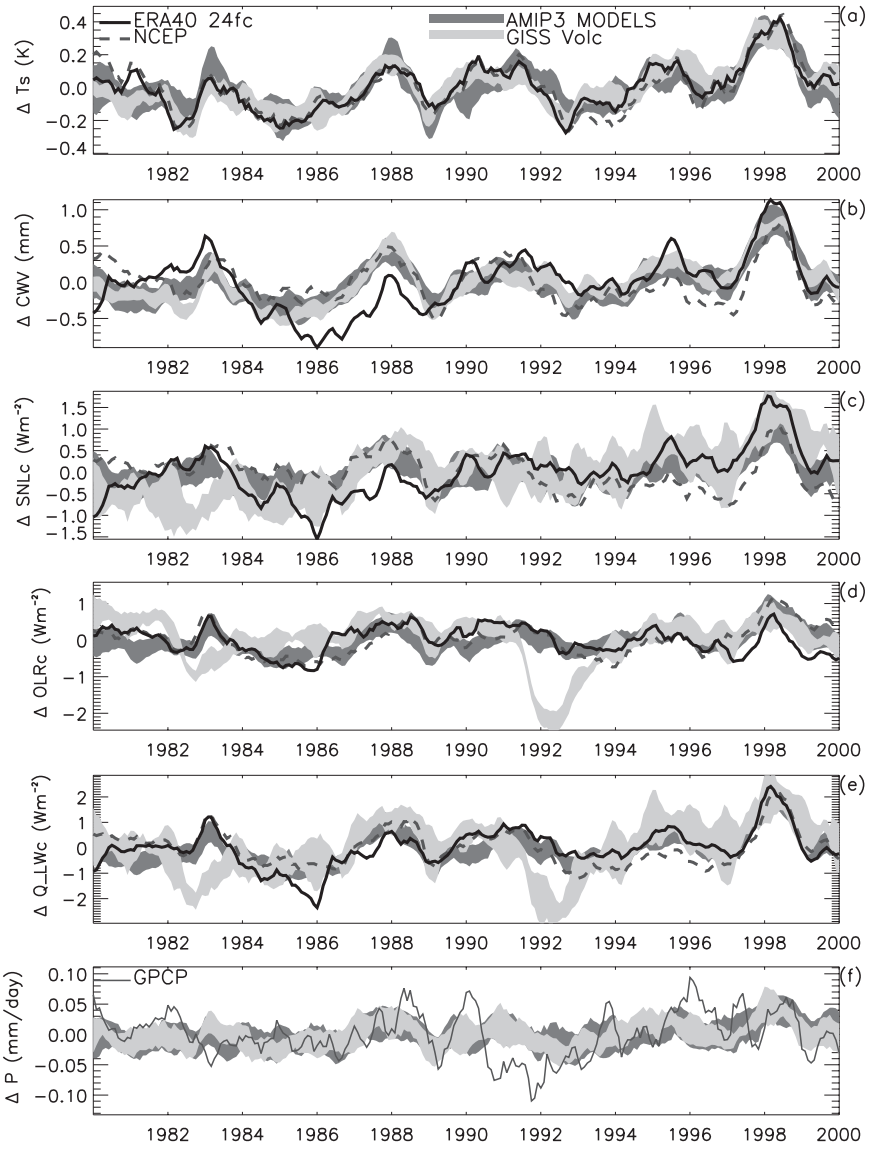

FIG. 2. Deseasonalized global monthly-mean anomalies of (a) surface temperature, (b) column-integrated water vapor, (c) clear-sky surface net longwave radiation, (d) clear-sky outgoing longwave radiation, (e) clear-sky longwave radiative cooling of the atmosphere, and (f) precipitation for reanalyses, GPCP precipitation, and AMIP3 models. The shading denotes the model ensemble mean ± one std dev where volcanic forcing is not included (dark shading) and is included (light shading) in two sets of ensembles. A 4-month smoothing is applied to all datasets.

denote statistically significant correlation at the 95% level allowing for autocorrelation.

There is a close correspondence between anomalies in CWV and T_s, which are dominated by El Niño–Southern Oscillation (ENSO), although individual models exhibit a range of sensitivities ~1–2.5 mm K^{-1} (Fig. 3a). Using the model ensemble mean values in Fig. 3 and Table 2, percentage changes in CWV with warming range from 6.7% K^{-1} for the CMIP3 model ensemble with volcanic forcing to 8.4% K^{-1} for the AMIP3 ensemble, close to that expected from the Clausius–Clapeyron equation and consistent with previous studies (Soden et al. 2005; Wentz et al. 2007).

A robust relationship between clear-sky surface net longwave radiation (SNLc) and CWV anomalies of 1–1.5 W m^{-2} mm^{-1} is apparent in Figs. 2–3. Combined with positive $d\text{CWV}/dT_s$, this translates to a statistically significant relationship between SNLc and T_s; specifically, the efficiency at which the surface can cool in the clear-sky longwave spectrum diminishes with warming.

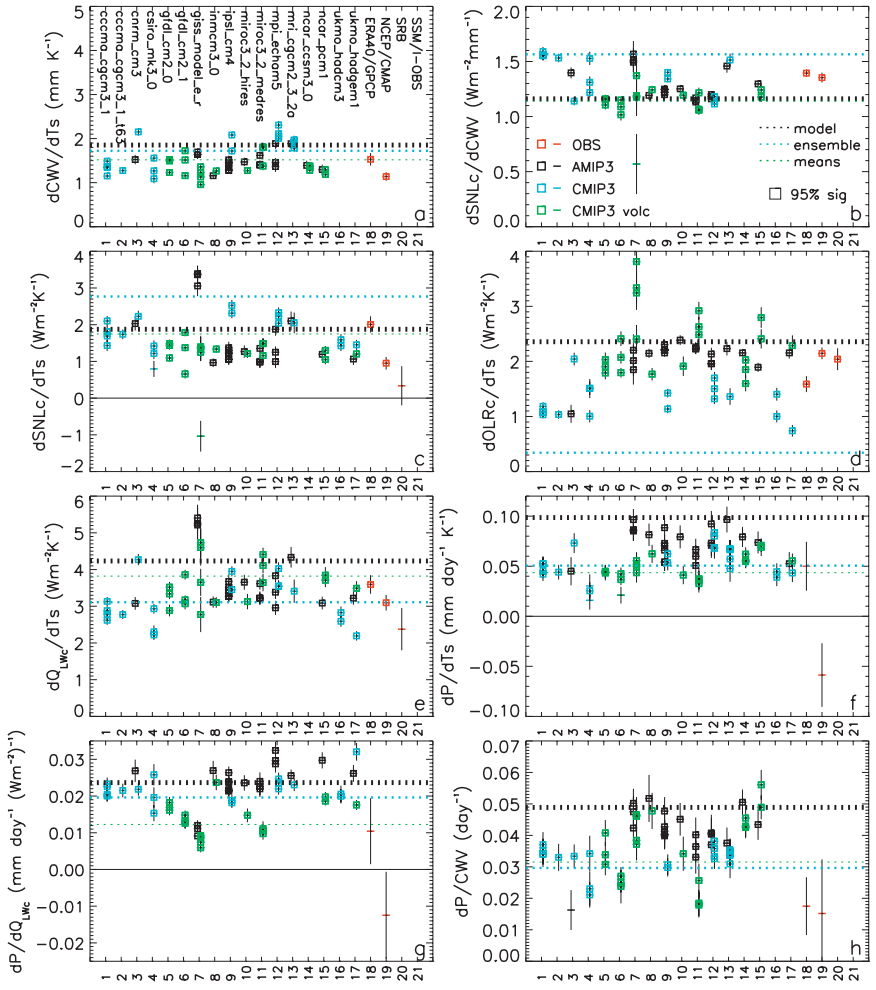

FIG. 3. Least squares linear fits between selected global-mean variables for models, reanalyses, and observations. Boxes denote significant correlation at the 95% confidence level. Horizontal dashed lines denote the model ensemble mean fit where statistically significant. Vertical lines denote ± one standard error in the linear fit.

This is the case for all models apart from run1 of GISS-ER. The SRB data also fail to show a statistically significant correlation for $d\text{SNLc}/dT_s$ because of spurious changes in land surface temperature (Allan 2007).

There is a positive trend in SNLc (Fig. 2c); this is more coherent when considering the ensemble mean of the CMIP3 models (not shown) since the variability relating to ENSO is essentially removed. The CMIP3 trend of 0.5 W m^{-2} decade^{-1} is consistent with values estimated over land by Wild et al. (2008) but is offset by increased clear-sky shortwave heating of the atmosphere (Q_{SWc}), which rises at the rate 0.2 W m^{-2} decade^{-1}, primarily because of moistening. This is discussed further in section 4.

Changes in T_s combined with invariant relative humidity result in a positive relationship between OLRc and T_s of order 2 W m^{-2} K^{-1} (e.g., Allan 2006), and this is consistent with results from NCEP, SRB, and the AMIP3 ensemble mean (Fig. 3d). The Centre National de Recherches Météorologiques (CNRM) AMIP experiment and ERA-40 reanalyses produce lower sensitivities, partly because greenhouse gas forcing was applied to these experiments; since greenhouse gas increases reduce OLRc and are positively coupled over decadal time scales with T_s, this acts to mask the positive direct relationship between T_s and OLRc (e.g., Slingo et al. 2000). In other words, the forcing is mixed with the feedback signal as diagnosed by OLRc. Similarly, other forcing agents that affect directly the OLRc, such as volcanic aerosols, will also impact the relationship between OLRc and T_s (e.g., Allan et al. 2003) and explain why the forced CMIP3 experiments do not produce a coherent relationship for $d\text{OLRc}/dT_s$. The CMIP3 models with volcanic forcings tend to show a higher sensitivity than the CMIP3 models without this forcing,

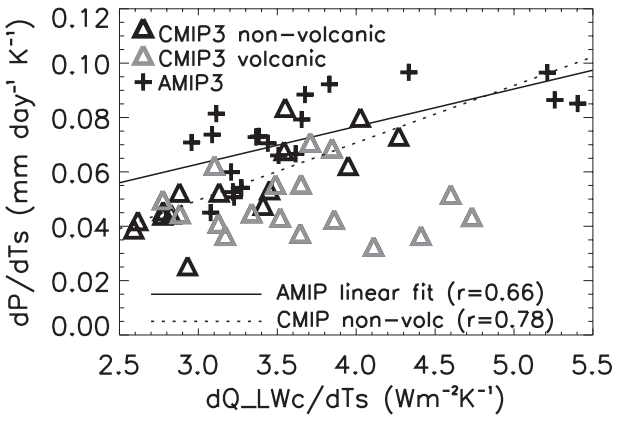

FIG. 4. Global-mean relationship between model-calculated dQ_{LWc}/dT_s and dP/dT_s.

caused by the large negative perturbations to OLRc following the El Chichon and Mount Pinatubo eruptions in 1982 and 1991. When the periods 1982–83 and 1991–93 are excluded, dOLRc/dT_s is comparable between volcanic and nonvolcanic CMIP3 experiments (not shown).

The increased clear-sky longwave cooling of the atmosphere to space and to the surface with rising temperature combine to produce a robust increase in Q_{LWc} with T_s, ranging from 3.1 to 4.2 W m^{-2} K^{-1} for the model ensemble means and reanalyses. The GISS-ER model produces a larger spread of sensitivities compared to the other models. The SRB data do not give a statistically significant correlation, relating to the spurious longer-term changes in SNLc over land. Nevertheless, the robust relationship between Q_{LWc}, T_s, and CWV implies a rise in mean precipitation with warming and moistening (e.g., Trenberth et al. 2003; Lambert and Webb 2008) as indicated by the models (Figs. 3f–h).

There is significant correlation between precipitation and Q_{LWc} for the model experiments (Fig. 3g), suggesting that changes in atmospheric clear-sky radiative cooling are important in determining changes in precipitation on a global scale. This is confirmed for the AMIP3 simulations and the CMIP3 model experiments that do not contain volcanic forcing: Fig. 4 shows that models with higher dQ_{LWc}/dTs correspond to a larger precipitation response to warming. Were Q_{LWc} changes to exactly balance the latent heating through precipitation,

$$dP \sim \frac{dQ_{\mathrm{LWc}}}{\rho_w L} \tag{1}$$

(ρ_w is water density; $L = 2.5 \times 10^6$ J kg^{-1}), then precipitation will increase at ~0.035 mm day^{-1} per W m^{-2} increase in Q_{LWc}. This is at the upper range of the dP/dQ_{LWc} calculated for the models.

The AMIP3 ensemble mean precipitation response is substantially larger than the CMIP3 ensembles. One explanation is that the response to ENSO is averaged out in the CMIP3 ensemble and the longer-term response to the smaller decadal warming trend is less coherent. However, this does not explain why individual CMIP3 models tend to simulate a smaller precipitation response compared to individual AMIP3 models. A more plausible explanation is that additional forcings applied in the CMIP3 experiments, such as greenhouse gases, directly influence the hydrological cycle through radiative heating of the troposphere (e.g., Yang et al. 2003), thereby lowering the calculated precipitation response to changes in T_s and CWV. This is backed up by the CNRM AMIP3 experiment, which also has a smaller precipitation response and is the only AMIP3 experiment to contain greenhouse gas forcing. An associated effect has recently been identified by Gregory and Webb (2008) to apply to cloud feedback.

A statistically significant response of P to T_s, Q_{LWc}, or CWV is not found for the ERA-40–GPCP and NCEP–CMAP combinations; changes in the observing system affect the integrity of these records (e.g., Yin et al. 2004). The larger monthly variability in GPCP precipitation following the introduction of SSM/I data is

TABLE 3. Annual-mean clear-sky radiation, water vapor, and precipitation over tropical oceans for AMIP3 climate models, 1980–2000.

Model	T_s (K)	CWV (mm)	SNLc (W m^{-2})	Q_{LWc} (W m^{-2})	OLRc (W m^{-2})	P (mm day^{-1})
CNRM.CM3.RUN1	299.20	42.34	−64.75	228.25	293.00	4.64
GISS.MODEL.E.R.RUN2	299.11	39.46	−75.50	209.95	285.45	4.09
INMCM3.0.RUN1	299.11	35.23	−74.43	210.39	284.82	3.81
IPSL.CM4.RUN1	299.24	36.92	−87.21	206.16	293.38	3.13
MIROC3.2.HIRES.RUN1	299.23	34.06	−84.06	204.66	288.72	3.43
MIROC3.2.MEDRES.RUN1	299.26	36.11	−81.24	204.45	285.69	3.32
MPI.ECHAM5.RUN1	299.25	39.86	−69.52	213.17	282.69	3.82
MRI.CGCM2.3.2A.RUN1	299.26	35.42	−77.69	201.59	279.28	3.34
NCAR.CCSM3.0.RUN1	299.25	37.45	—	—	288.78	3.68
NCAR.PCM1.RUN1	299.17	35.98	−80.13	211.31	291.43	4.14
UKMO.HADGEM1.RUN1	299.29	—	−73.22	218.15	291.36	4.00

TABLE 4. Annual-mean clear-sky radiation, water vapor, and precipitation over tropical oceans for CMIP3 climate models, 1980–2000.

Model	T_s (K)	CWV (mm)	SNLc (W m^{-2})	Q_{LWc} (W m^{-2})	OLRc (W m^{-2})	P (mm day^{-1})
CCCMA.CGCM3.1.RUN2	298.96	33.68	−83.73	204.04	287.77	3.65
CCCMA.CGCM3.1.T63.RUN1	298.66	33.16	−83.20	204.79	287.99	3.67
CNRM.CM3.RUN1	297.82	37.57	−69.95	220.01	289.97	4.28
CSIRO.MK3.0.RUN1	298.10	34.45	−79.56	209.11	288.66	3.16
GFDL.CM2.0.RUN1	298.44	33.68	−75.11	206.30	281.42	3.50
GFDL.CM2.1.RUN1	298.86	35.33	−73.19	209.16	282.35	3.83
GISS.MODEL.E.R.RUN2	299.15	39.28	−75.91	209.37	285.28	4.02
INMCM3.0.RUN1	298.15	33.08	−77.99	205.55	283.54	3.84
IPSL.CM4.RUN1	299.52	37.85	−86.65	207.09	293.74	3.19
MIROC3.2.HIRES.RUN1	298.74	32.39	−85.81	203.08	288.88	3.43
MIROC3.2.MEDRES.RUN1	298.32	33.42	−84.41	199.38	283.79	3.22
MPI.ECHAM5.RUN1	299.51	40.52	−68.67	213.78	282.45	3.87
MRI.CGCM2.3.2A.RUN1	298.78	33.67	−79.60	198.39	277.99	3.19
NCAR.CCSM3.0.RUN1	298.99	36.49	—	—	287.94	3.63
NCAR.PCM1.RUN1	298.84	35.25	−80.73	210.38	291.11	4.24
UKMO.HADCM3.RUN1	299.49	—	−72.41	211.95	284.35	3.80
UKMO.HADGEM1.RUN1	298.27	—	−76.16	213.44	289.60	3.85

apparent in Fig. 2f as previously documented by Quartly et al. (2007).

4. Tropical comparison

Concentrating now on the tropics (30°S–30°N) allows the simulated relationships to be evaluated against available observations.

a. Tropical ocean mean quantities

Tables 3–5 show tropical ocean mean quantities over the period 1980–2000 for individual models, model ensembles, reanalyses, and observational estimates, where available. The models that overestimate CWV compared with SSM/I (CNRM, ECHAM5) most closely reproduce the SNLc from ERA-40 and the

TABLE 5. Tropical ocean annual-mean clear-sky radiation, water vapor, and precipitation for reanalyses, satellite observations, and climate model ensemble mean, 1980–2000.

	T_s (K)	CWV (mm)	SNLc (W m^{-2})	Q_{LWc} (W m^{-2})	OLRc (W m^{-2})	P (mm day^{-1})
ERA-40–GPCP	298.28	37.33	−71.92	215.86	287.77	2.97
NCEP–CMAP	299.21	36.12	−76.71	213.48	290.19	3.60
SRB	298.63	—	−76.26	214.02	290.28	—
ERBS–CERES–Prata–SSM/I	299.10	37.33	−64.30	224.15	288.66	2.86
AMIP ensemble	299.22	35.55	−80.93	205.45	286.38	3.41
CMIP ensemble nonvolcanic	298.87	36.08	−78.63	208.02	286.65	3.64
CMIP ensemble volcanic	298.61	34.53	−78.74	205.47	284.21	3.64
Ascent						
ERA-40–GPCP	299.83	45.15	−63.30	220.04	283.34	5.07
NCEP–CMAP	300.79	42.07	−70.88	216.22	287.10	6.22
SRB	300.22	—	−69.51	215.81	285.32	—
ERBS–CERES–Prata–SSM/I	300.72	45.35	−54.92	231.85	286.97	5.31
AMIP ensemble	300.66	43.68	−72.78	208.37	281.15	6.57
CMIP ensemble nonvolcanic	300.34	45.07	−69.85	211.37	281.22	6.88
CMIP ensemble volcanic	300.20	43.14	−70.69	208.03	278.75	7.16
Descent						
ERA-40–GPCP	296.95	30.59	−79.36	212.23	291.59	1.19
NCEP–CMAP	297.84	30.99	−81.75	211.09	292.84	1.33
SRB	297.26	—	−82.12	212.44	294.57	—
ERBS–CERES–Prata–SSM/I	297.74	30.70	−72.23	217.66	290.08	0.77
AMIP ensemble	298.26	30.13	−86.37	203.51	289.87	1.31
CMIP ensemble nonvolcanic	297.86	29.85	−84.71	205.70	290.42	1.41
CMIP ensemble volcanic	297.60	29.06	−83.87	203.81	287.68	1.42

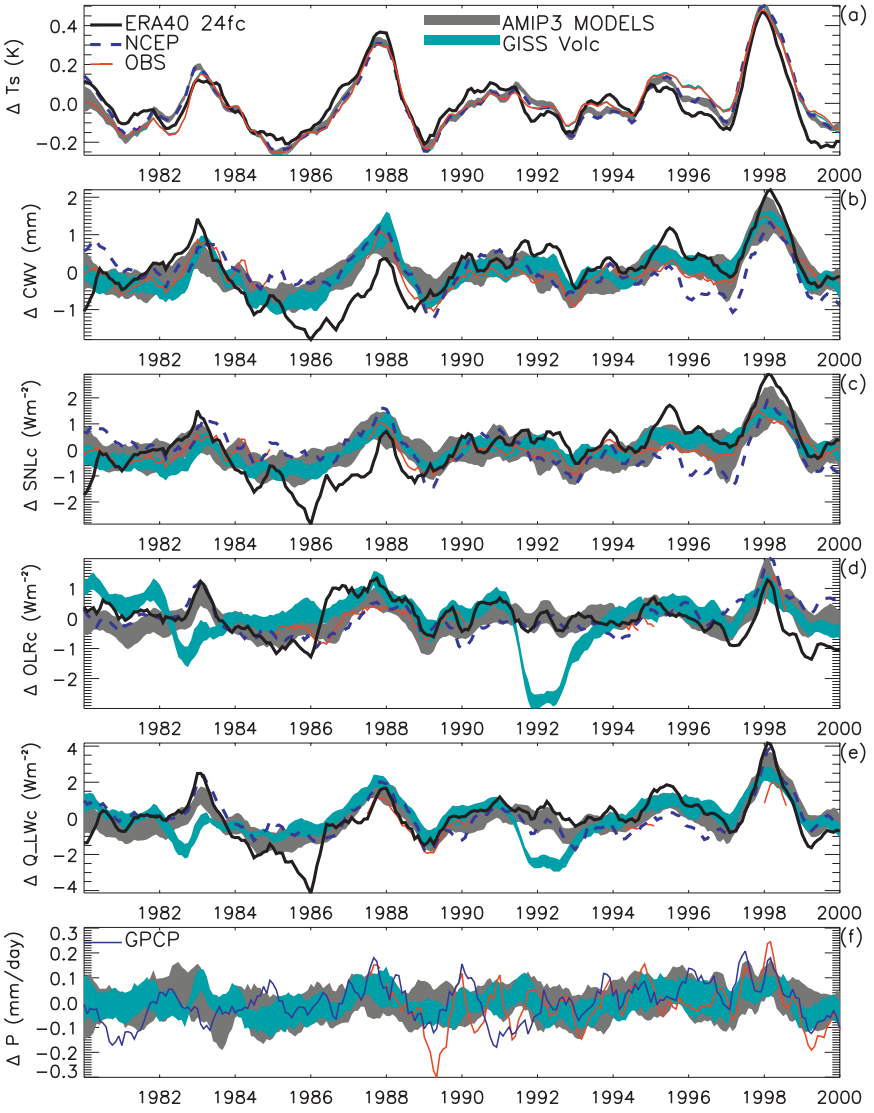

FIG. 5. As in Fig. 2 but for the tropical oceans (30°S–30°N) and also including observational estimates.

SSM/I observationally based estimate. The model ensemble mean SNLc of ~ -80 W m^{-2} is close to NCEP and SRB estimates but more negative than ERA-40 and the SSM/I observationally derived estimate. Wild (2008) also found that climate models underestimated surface downwelling longwave fluxes. Most models underestimate Q_{LWc} compared to reanalyses and the observationally derived estimate [e.g., Model for Interdisciplinary Research on Climate (MIROC), MRI CGCM2]. There is a large range of observed precipitation values: CMAP estimates the highest precipitation totals (3.6 mm day^{-1}) and SSM/I and GPCP the lowest at just under 3 mm day^{-1} giving a range of around 20%.

b. *Variability over the ocean*

As for the global comparisons, there is close correspondence between T_s, CWV, and SNLc changes for each dataset with positive anomalies during warm El Niño months (Figs. 5a–c). The variability in OLRc (Fig. 5d) appears less coherent since positively coupled temperature and moisture anomalies exert contrasting effects on top of atmosphere longwave emission. In addition, the direct effect of El Chichon and Mount Pinatubo on OLRc is apparent in the GISS-ER ensemble but not in the remaining models or the reanalyses, which did not prescribe volcanic aerosol. Despite remaining inhomogeneities in the ERA-40 24-h forecasts

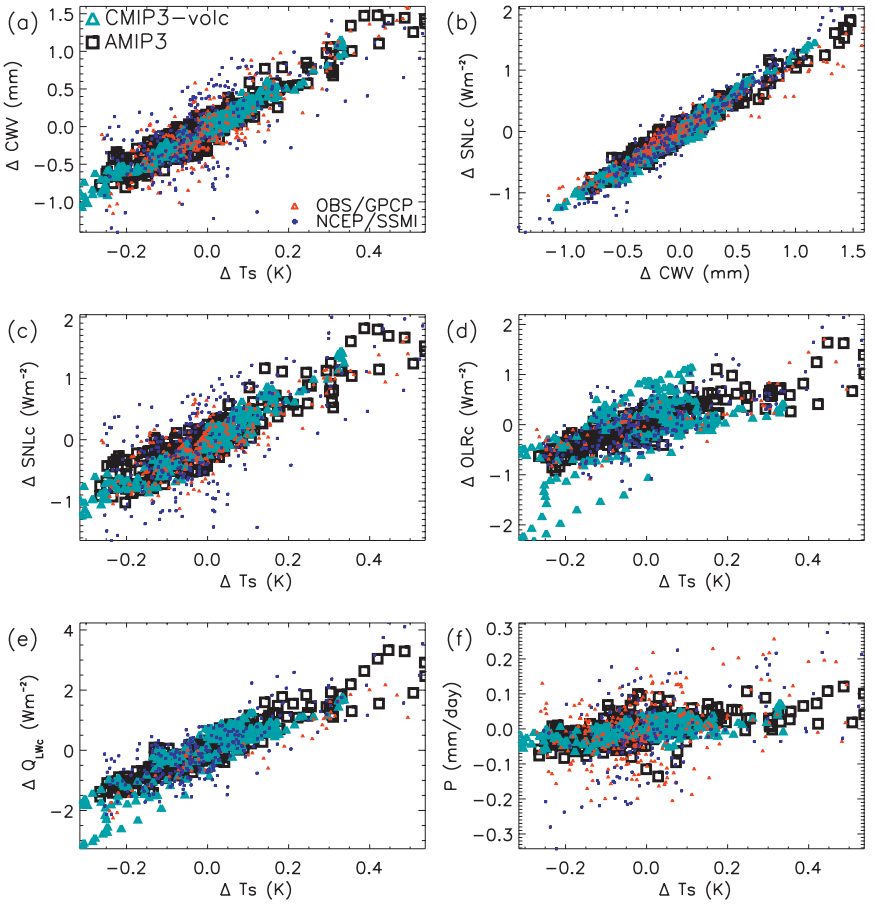

FIG. 6. Scatterplot for selected variables for the AMIP3 nonvolcanic ensemble mean, the CMIP3 volcanic forcing ensemble mean, observationally derived datasets, and NCEP–SSM/I over the period 1980–2000.

(e.g., 1985–86), variability in Q_{LWc} is generally consistent between datasets and models (Fig. 5e), which is partly explained by the fact that humidity errors through the column have opposing effects on radiative cooling to the surface and to space (Allan 2006). The interannual variability in precipitation (Fig. 5f) is small compared to the model ensemble spread and less coherent than the other variables analyzed.

Relationships between the variables shown in Fig. 5 are displayed as scatterplots in Fig. 6 and linear fits in Fig. 7. The generally larger scatter apparent in the observations and reanalyses compared to the models in Fig. 6 primarily reflects the smoothing introduced in constructing model ensemble means. Departures from the linear relationships in Fig. 6 also indicate time-scale-dependent responses of the system to volcanic forcings or ENSO variability as discussed by Harries and Futyan (2006).

The AMIP3 ensemble mean, CMIP3 volcanic ensemble mean, ERA-40 and SSM/I–HadISST datasets all produce a robust relationship between CWV and T_s of ~3 mm K^{-1} (Fig. 6a). The NCEP data produce a lower sensitivity, relating to the negative trend in CWV relative to the other datasets (Fig. 5b). Individual ensemble members provide a substantial scatter in $d\mathrm{CWV}/dT_s$ ranging from 2.2 to 4.0 mm K^{-1} (Fig. 7a). Part of this scatter appears to relate to unpredictable fluctuations since there is substantial spread (of order 1 mm K^{-1}) between ensemble members of individual models. The MIROC high-resolution CMIP3 experiment simulates the lowest sensitivity of all models, partly because of underestimation in mean CWV (Table 4).

As for the global comparison, the dSNLc/dCWV sensitivity is robust between models and reanalyses (Fig. 7b), ranging from about 1 to 1.4 W m^{-2} mm^{-1}. The CMIP3 models without volcanic forcing lie at the upper end of this range; since greenhouse gas increases enhance the atmospheric cooling to the surface by 0.12 W m^{-2} $decade^{-1}$ over the period 1980–2000 (Allan 2006), and the increases are concurrent with trends in CWV of 0.43 mm $decade^{-1}$, the sensitivity dSNLc/dCWV

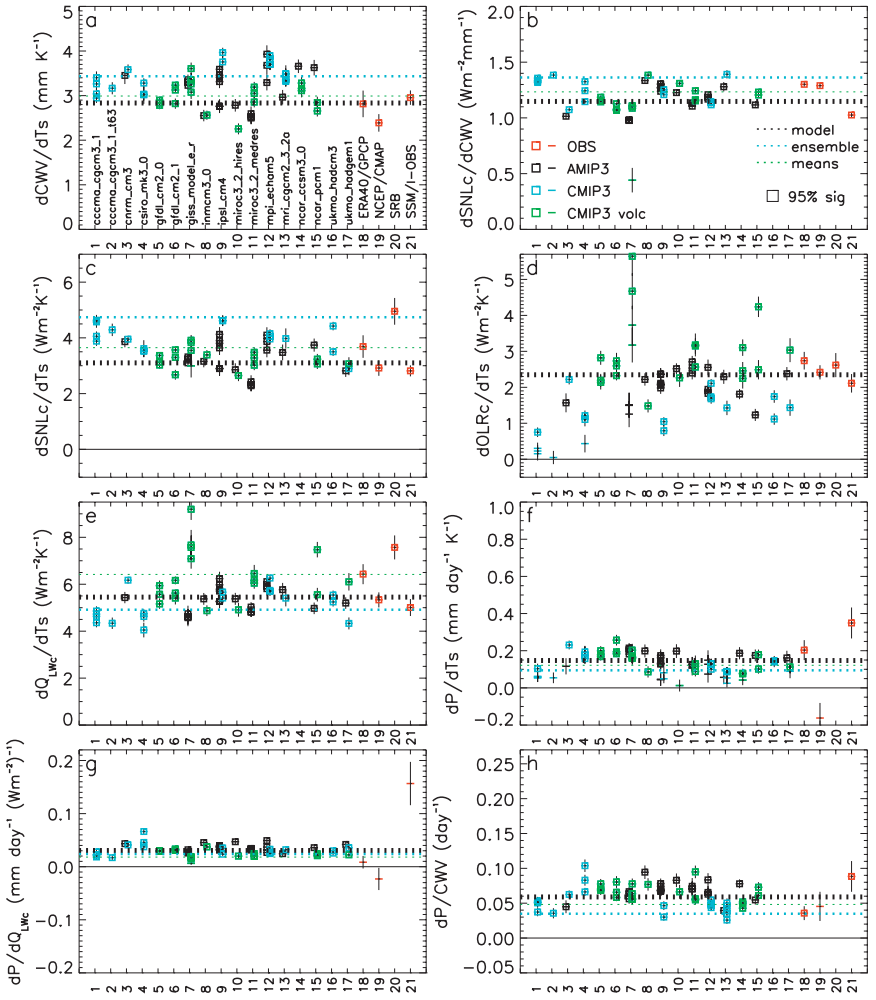

FIG. 7. As in Fig. 3 but for the tropical oceans and also considering the observationally based datasets.

is enhanced by the factor $0.12/0.43 = 0.28$ W m^{-2} mm^{-1}, explaining why the CMIP3 nonvolcanic ensemble mean sensitivity is larger than the AMIP3 ensemble mean. The CMIP3 ensemble mean containing volcanic forcings produces a similar sensitivity to the AMIP3 ensemble because the volcanic forcing acts to reduce the correspondence between changes in CWV and increases in greenhouse gases. The observational estimate of dSNLc/dCWV is based upon a fit to surface radiometric observations (Prata 1996), which takes no account of changes in greenhouse gases or volcanic forcings and this falls at the lower end of the range (1 W m^{-2} mm^{-1}).

There is a positive relationship between SNLc and T_s (Fig. 6c) but with a large spread (2–5 W m^{-2} K^{-1}; Fig. 7c); the CMIP3 nonvolcanic ensemble mean and SRB data are at the upper end of this range. A robust trend in CMIP3 nonvolcanic ensemble mean SNLc of 0.71 W m^{-2} K^{-1} (Fig. 8a) is larger than the global trend and the AMIP3 ensemble. This is offset by increased clear-sky shortwave heating (Q_{SWc}) of 0.26 W m^{-2} K^{-1} (Fig. 8b). To understand these trends further, radiative calculations were performed on a tropical mean profile subject to a tropospheric warming of 1 K with constant relative humidity and to greenhouse gas increases from 1980 levels to 2000 concentrations (Fig. 8c; for further details see Allan 2006). Depending on the tropical ocean warming trend (0.1 or 0.15 K decade^{-1}), the increases in OLRc due to the warming are more than compensated by the increased absorption by greenhouse gases (e.g., Slingo et al. 2000). Therefore, increases in Q_{LWc} are determined primarily by increased SNLc because of the warming, moistening, and greenhouse gas increases. The overall rate of increase in Q_{LWc} of 5.3 W m^{-1} K^{-1} is offset by greenhouse gas increases by 1.5 W m^{-1} K^{-1} (assuming a tropical warming trend of 0.15 K decade^{-1}) and further by

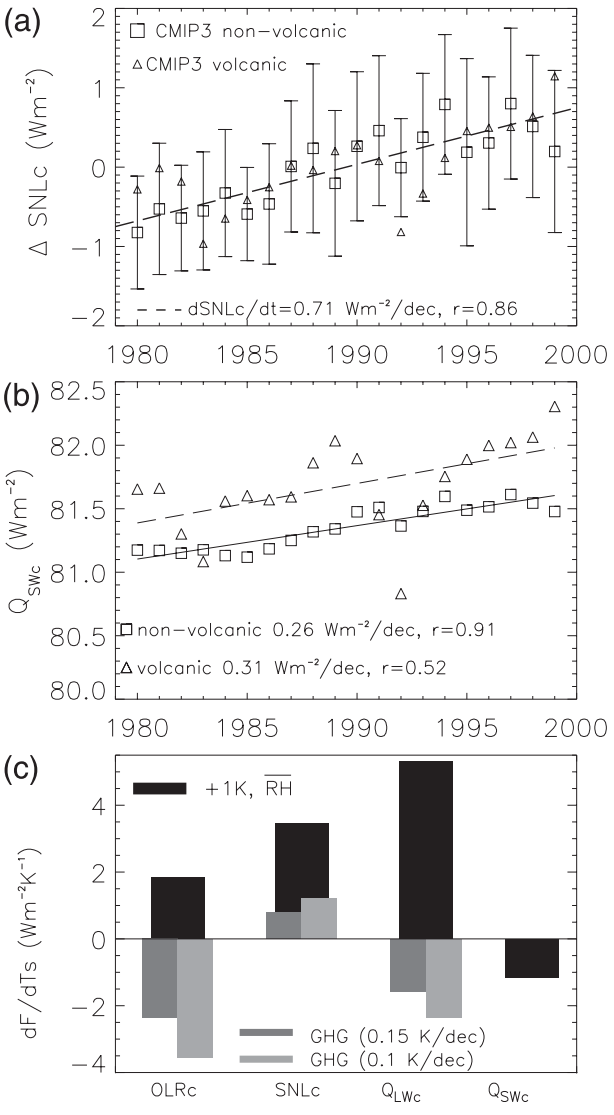

FIG. 8. (a) Global–annual-mean anomalies of clear-sky surface net longwave radiation from CMIP3 model ensemble means (for the models without volcanic forcings; error bars denote one std dev of the monthly-mean anomalies and a trend line is also plotted), (b) Global–annual-mean clear-sky atmospheric shortwave absorption (Q_{LWc}) from CMIP3 model ensemble means, and (c) sensitivity of tropical mean radiative fluxes in response to a 1-K increase in tropospheric temperatures and 1980–2000 change in greenhouse gases assuming a range in temperature trend.

enhanced Q_{SWc} because of water vapor by 1.1 W m^{-2} K^{-1} leading to an overall increase in total clear-sky radiative cooling of 2.7 W m^{-2} K^{-1}, similar to the global estimate used by Allen and Ingram (2002).

A positive sensitivity, dOLRc/dT_s = 2.3 W m^{-2} K^{-1}, is calculated for the AMIP3 ensemble mean, broadly consistent with the reanalyses and satellite data (Fig. 7d). The nonvolcanically forced CMIP3 models tend to simulate a smaller sensitivity since the interannual relationships between OLRc and T_s are averaged out in the ensemble mean and the longer-term response of OLRc to warming is to a large extent canceled out by the impact of the concurrent rises in greenhouse gases (Fig. 8c). The volcanically forced CMIP3 models produce a higher sensitivity because of the rapid drop in OLRc in response to the direct effect of volcanic aerosols relative to the slower decline in T_s in response to the negative net radiative forcing.

All datasets considered produce a robust increase in Q_{LWc} with T_s over the tropical oceans (Figs. 6–7d). The AMIP3 ensemble mean dQ_{LWc}/dT_s is 5.5 W m^{-2} K^{-1}, with about 60% resulting from extra net cooling to the surface and 40% to the enhanced OLRc with warming. For the nonvolcanic CMIP3 ensemble mean, dQ_{LWc}/dT_s is lower and exclusively explained by the positive response of SNLc to surface warming, as expected from the theoretical calculations in Fig. 8c. Conversely, the direct impact of the volcanic forcing on OLRc for the CMIP3 volcanic ensemble mean adds to the positive dSNLc/dT_s relationship, producing the largest sensitivity, dQ_{LWc}/dT_s = 6.7 W m^{-2} K^{-1}. The CMIP3 GISS-ER model produces the largest sensitivity, explained by the large calculated sensitivity dOLRc/dT_s, albeit with large scatter.

The majority of models indicate a positive precipitation response to surface warming (Fig. 7f) with ensemble mean sensitivity of 0.1–0.15 mm day^{-1} K^{-1}. The GPCP data indicate a larger response of 0.2 ± 0.05 mm day^{-1} K^{-1} but are within the range of the individual model spread. The SSM/I data produced the largest sensitivity of 0.35 ± 0.1 mm day^{-1} K^{-1}, while the CMAP data produce a statistically insignificant negative relationship. The model ensemble means produce a significant sensitivity dP/dQ_{LWc} of ~0.02–0.03 mm day^{-1}(W m^{-2})$^{-1}$, slightly smaller than expected by the balancing of latent heating through precipitation with clear-sky longwave radiative cooling [see Eq. (1)]. Again the reanalyses/observations do not produce a significant statistical relationship. The model ensemble mean linear fit, dP/dCWV = 0.035–0.06 day^{-1}, is consistent with the ERA-40–GPCP and NCEP–CMAP sensitivity (Fig. 7g). However, it should be noted that NCEP CWV and CMAP precipitation are both subject to possibly spurious negative trends, so the agreement in terms of dP/dCWV may be somewhat fortuitous. The SSM/I-derived sensitivity of 0.09 ± 0.02 day^{-1} is larger than the model ensemble means but within the spread of the individual model sensitivities.

c. Ocean ascending and descending regimes

Analysis is now conducted separately for the ascending and descending branches of the tropical ocean using 500-hPa vertical motion fields (ω). Mean upward

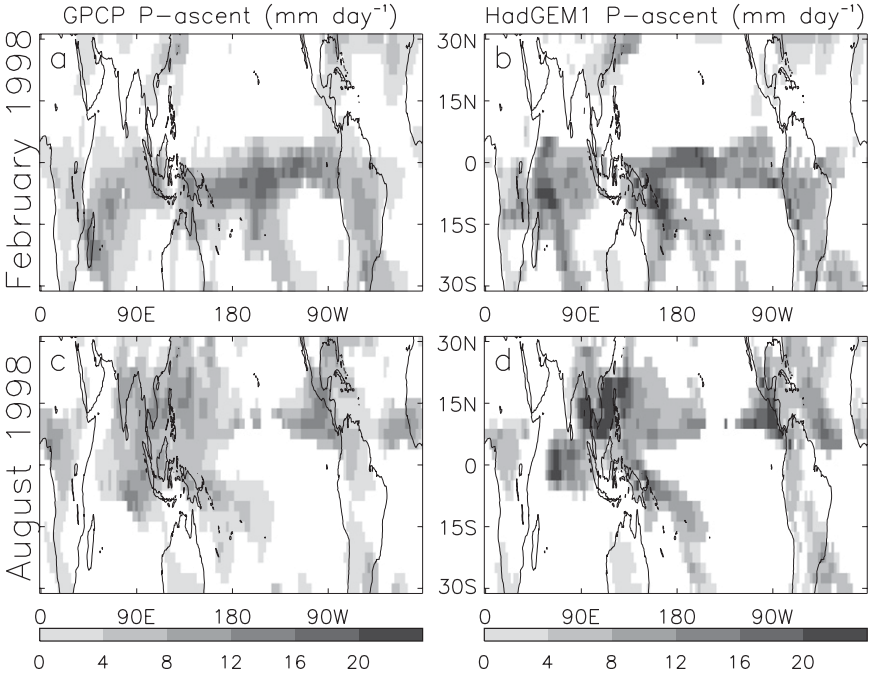

FIG. 9. Ascent region precipitation (mm day^{-1}) for (left) GPCP and (right) HadGEM1 AMIP3 experiment for (top) February and (bottom) August 1998.

and downward motion is calculated each month using each model's ω to subsample its corresponding diagnostics and using reanalysis ω to subsample the reanalyses/observations (Allan and Soden 2007). This is illustrated for the GPCP and HadGEM1 AMIP3 ascending region precipitation fields for February and August 1998 in Fig. 9. Sensitivities are displayed for the ascending (Fig. 10) and descending (Fig. 11) regions of the tropical oceans.

There is substantial scatter of ascent region $d\text{CWV}/dT_s$ between models, reanalyses, and observations, covering the range 3–5 mm K^{-1} (Fig. 10a). However, all model ensemble means considered produce a rise of ~9% K^{-1}, in agreement with the HadISST–SSM/I observations and consistent with the rate expected from Clausius–Clapeyron plus moist adiabatic adjustment (Wentz et al. 2007). For the descent regions (Fig. 11a), a lower sensitivity is simulated as expected from the smaller mean CWV. Normalizing by mean CWV, both CMIP3 ensemble means produce a similar relative rise in water vapor with warming (8.2% K^{-1}) although the AMIP3 ensemble mean, reanalyses, and observations are lower (5.6%–5.8% K^{-1}), slightly lower than expected from the Clausius–Clapeyron relationship.

The relationship between SNLc and CWV is slightly stronger, although with more scatter, for the drier, descent regions (Fig. 11b) than the ascent regions, reflecting the saturation of water vapor continuum absorption with increased moisture (e.g., Prata 1996). The relationship for the GISS-ER model run1 over descending regions is unrealistically low, suggesting that the diagnostic error is manifest most strongly in these regions.

The sensitivity $d\text{SNLc}/dT_s$ is larger for the ascent regimes (3–5.5 W m^{-2} K^{-1}) than for descent regions (1.5–4 W m^{-2} K^{-1}), which is explained by the differing responses in moisture. The CMIP3 model ensemble means and SRB data produce a higher $d\text{SNLc}/dT_s$ for the descent regions (3–4 W m^{-2} K^{-1}) compared with the AMIP3 ensemble, reanalyses, and SSM/I-derived estimates of around 2 W m^{-2} K^{-1}.

The OLRc response to warming is smaller for the ascending region than the descending regions. The ERA-40 data simulate a significant negative ascent region OLRc trend over the period 1980–2000 (−0.8 W m^{-2} decade^{-1}), with particularly negative anomalies in 1999, corresponding with anomalously low T_s (not shown). The relationship with T_s for this region is not significant for ERA-40, NCEP, or ERBS–CERES; a statistically significant relationship is produced by the AMIP3 ensemble mean (1.2 W m^{-2} K^{-1}) and SRB data (1.5 W m^{-2} K^{-1}). For the descent region, changes in OLRc show greater correlation with T_s; the AMIP3 ensemble mean, reanalyses, and observations have a sensitivity of about (2.5 W m^{-2} K^{-1}).

The combination of changes in SNLc and OLRc with T_s result in a robust relationship between Q_{LWc} and T_s

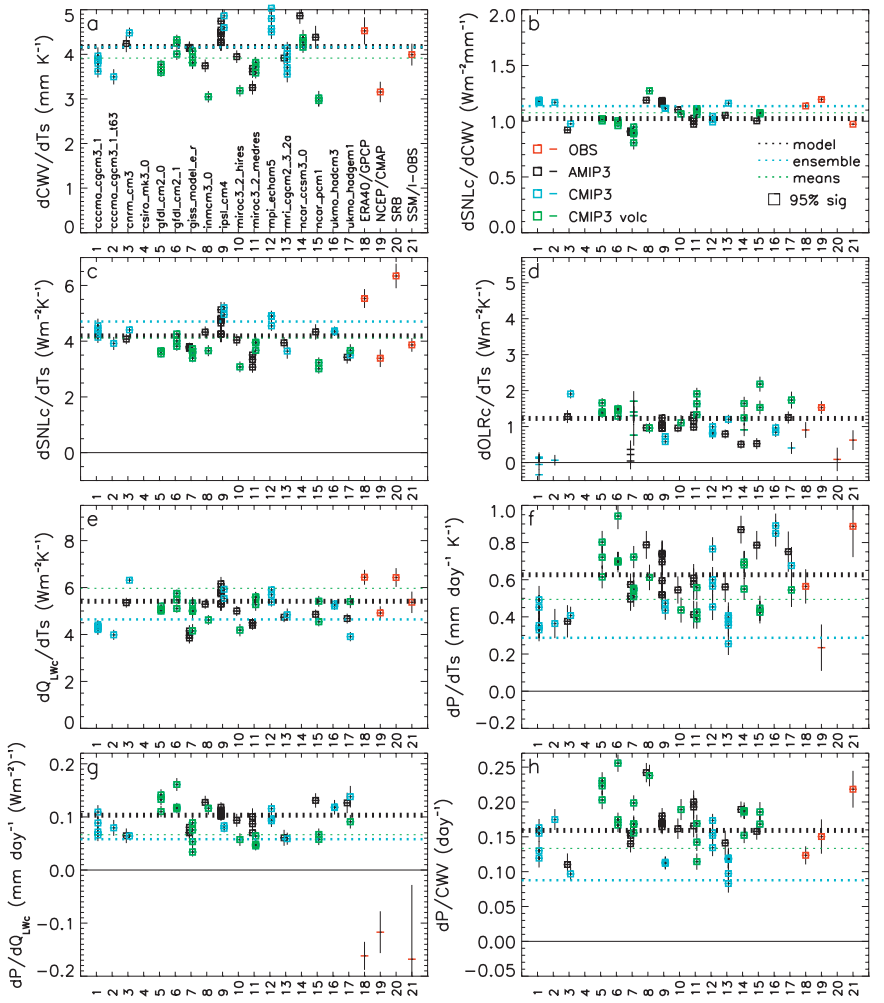

FIG. 10. As is Fig. 3 but for the tropical ocean ascent regions.

for both the ascending and descending branches of the tropical circulation. Since the descending regime contains less cloud, the clear-sky relationships here are particularly relevant and more directly comparable to the cloud-screened observations. The AMIP3 and CMIP3 nonvolcanic ensembles and the NCEP data and observationally derived estimates all produce an increase in Q_{LWc} with T_s of around 4–5 W m^{-2} K^{-1} for both regimes. The CMIP3 volcanic ensemble produces a larger sensitivity of order 6 W m^{-2} K^{-1}, reflecting the direct effect of volcanic stratospheric aerosols that reduce both OLRc and T_s, obscuring the radiative–convective response to warming.

The precipitation response to warming is positive in the ascending regime (Fig. 10f), but with substantial scatter (0.2–1.0 mm day^{-1} K^{-1}) and the relationship is not statistically significant for the CMAP product. When normalizing by mean P, the CMIP3 model ensemble means simulate rises of around 6% K^{-1} while the AMIP ensemble mean and ERA-40–GPCP estimate is close to 10% K^{-1}; these values are broadly consistent with the Clausius–Clapeyron relationship and explained by the rises in moisture that supply the primarily convectively driven rainfall (e.g., Trenberth et al. 2003). However, the SSM/I–HadISST response is substantially larger at 18% K^{-1}.

Employing mean values from Table 5, the relationship between ascent region precipitation and CWV (Fig. 10h) can be converted to units of %/% as (dP/dCWV) (CWV/P). A 1:1 relationship is calculated, to within 0.07%/%, for the AMIP3 ensemble mean and the GPCP–ERA-40 and CMAP–NCEP combinations. A smaller response is calculated for the CMIP3 volcanic ensemble (0.8%/%) and CMIP3 nonvolcanic ensemble (0.7%/%), while a much larger response is calculated for the SSM/I dataset 1.6–2.0%/%. For the descent region, only the GISS-ER AMIP/CMIP and CNRM CMIP3 models simulate statistically significant (positive)

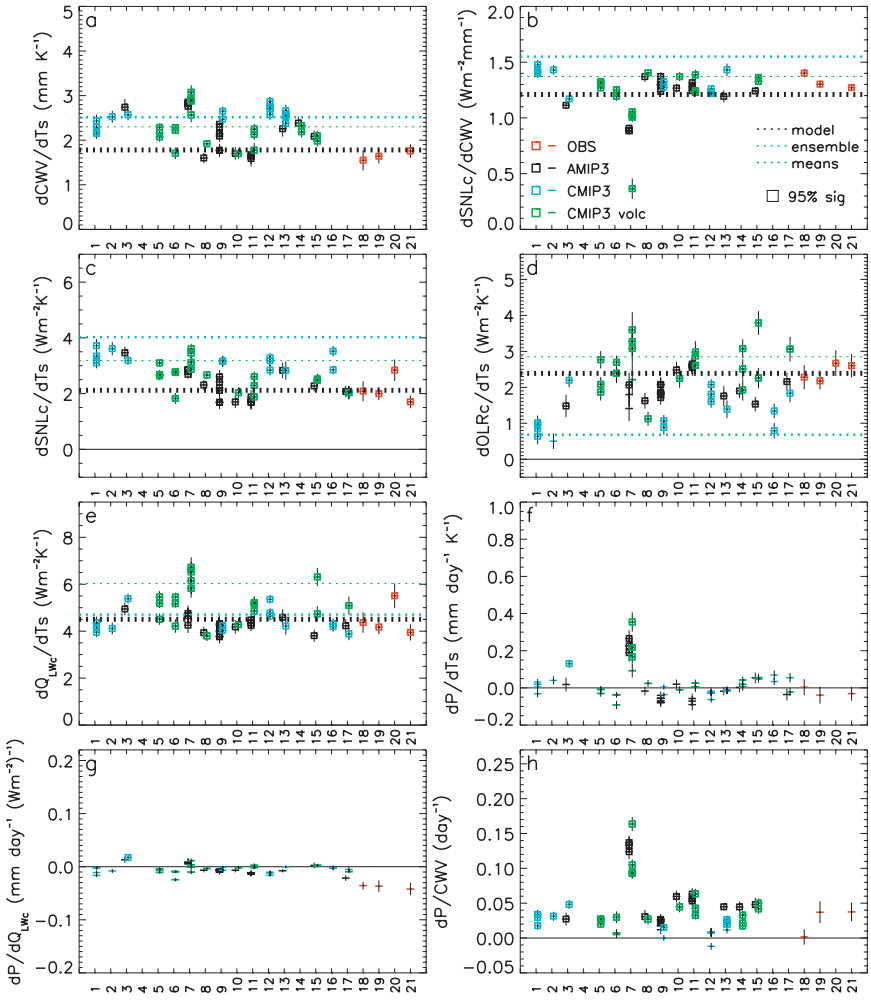

FIG. 11. As is Fig. 3 but for the tropical ocean descent regions.

responses (Fig. 11f). A weakly positive dependence of precipitation on CWV is simulated by the models for the descent region, while the observations do not produce a statistically significant relationship.

A robust positive relationship between precipitation and Q_{LWc} is calculated for the ascending regime but not the descending regime as expected. Since the tropical mean precipitation is driven by changes in the radiation balance but the ascent region precipitation changes are dominated by the enhanced moisture to compensate, changes in descending region precipitation are not expected to be positive (Trenberth et al. 2003). On an interannual time scale, changes in observed precipitation with Q_{LWc} and T_s are not well correlated. This is likely to be caused by the limited period in which the observationally derived estimates are calculated in addition to inconsistencies between datasets. However, Allan and Soden (2007) detected positive trends in observed precipitation over the ascent regions and negative trends over the descending regimes of the tropical circulation over the period 1979–2006 with a substantially larger magnitude trend in the observations than the models.

d. Variability over land

Over land, where surface water is limited, advection of moist air is required to maintain relative humidity with warming. Fig. 12 shows that a positive relationship between T_s and CWV exists for the AMIP3 models and reanalyses and consistent with surface humidity observations (Willett et al. 2008). However, the magnitude of the CWV response is smaller with the linear fit calculated from the model ensemble means and reanalyses lying in the range 3.9–5.4% K^{-1}, lower than that expected from the Clausius–Clapeyron equation. While the ensemble mean sensitivity of SNLc to CWV lies in the range 1.1–1.4 W m^{-2} mm^{-1}, in agreement with other regions, the lower CWV sensitivity to warming leads to

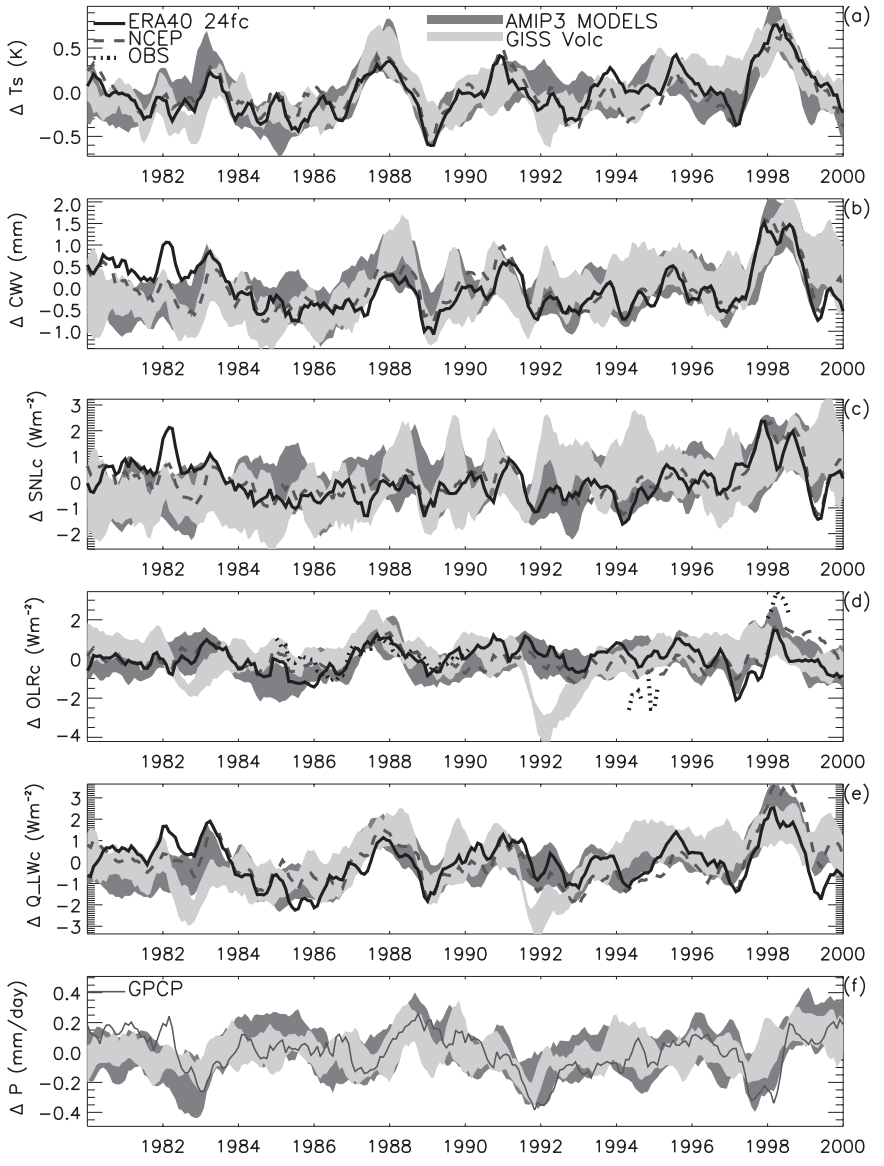

FIG. 12. As is Fig. 2 but for tropical land regions.

a less coherent relationship between SNLc and T_s than for the global mean or tropical oceans. Most models do not produce a statistically significant relationship, although the model ensemble means produce a robust relationship of ~1 W m^{-2} K^{-1} and a trend of around 0.5 W m^{-2} decade^{-1}, consistent with Wild et al. (2008).

The AMIP3 ensemble mean changes in OLRc are positively coupled to T_s, with a sensitivity of 2.2 W m^{-2} K^{-1}, in broad agreement with the ERA-40, NCEP, and SRB estimated values (1.7–2.2 W m^{-2} K^{-1}). The OLRc and SNLc response lead to a positive relationship between Q_{LWc} and T_s for the AMIP ensemble mean of order 3 W m^{-2} K^{-1}, lower than NCEP (3.5 W m^{-2} K^{-1}) but larger than ERA-40 (2.5 W m^{-2} K^{-1}). The SRB data (not shown) produce a spurious relationship between SNLc and T_s (Allan 2007), removing any statistically significant relationship between Q_{LWc} and T_s. Observed differences in OLRc from ERBS, ScaRaB, and CERES are within the expected calibration and sampling differences of 1 W m^{-2}, but this is similar to the magnitude of interannual variability.

Changes in precipitation over land are generally consistent between GPCP and the AMIP3 models with El Niño periods corresponding to negative anomalies (e.g., Gu et al. 2007). Since El Niño corresponds to warmer and moister conditions globally, contributing to higher precipitation rates, while the dynamical changes contribute to negative precipitation anomalies over land,

the relationship between precipitation and T_s over land is incoherent (Adler et al. 2008).

5. Conclusions

Links between clear-sky longwave radiation and aspects of the hydrological cycle were quantified in models, reanalyses, and observations over the period 1980–2000. There was broad consistency in relationships between variables in all datasets with low-level moistening explaining enhanced clear-sky radiative cooling of the atmosphere to the surface and enhanced precipitation in ascending regions of the tropical circulation. The GISS-ER model produced the least coherent relationships and CMAP precipitation, SRB surface fluxes, and moisture variability in ERA-40 appear spurious. The following are the primary conclusions:

- Models tend to underestimate the clear-sky surface net longwave radiation (SNLc), which is consistent with previous work (Wild 2008); only models that overestimate column-integrated water vapor (CWV) can reproduce SNLc derived semiempirically from observations [e.g., CNRM, Max Planck Institute (MPI)-ECHAM5]. Nevertheless, biases in mean fields do not necessarily impact climate feedbacks (John and Soden 2007).
- A robust increase in SNLc (less surface cooling) with CWV ($\sim 1-1.5$ W m^{-2} mm^{-1}) is relatively insensitive to region or dataset. Where greenhouse gas increases are prescribed and correlated with CWV increases, the calculated sensitivity is enhanced.
- A significant rise in CWV with warming was detected in all datasets with the largest response over tropical ocean ascending regions and smallest response over land regions.
- Increased radiative cooling of the atmosphere to the surface with warming is robust, of order 2–5 W m^{-2} K^{-1} over tropical oceans. The relationship over land is less coherent but a significant trend in SNLc was present for the CMIP3 ensemble mean of around 0.5 W m^{-2} decade^{-1} for tropical land and global means, consistent with analysis of surface observations over land (Wild et al. 2008); trends over tropical oceans are slightly larger.
- Changes in OLRc are sensitive to forcing from greenhouse gas increases and volcanic aerosol in addition to the response of the hydrological cycle to warming, consistent with previous studies (e.g., Slingo et al. 2000).
- A robust increase in clear-sky longwave radiative cooling of the atmosphere (Q_{LWc}) with warming applies to all regions and datasets considered. For models without volcanic forcings, Q_{LWc} increases at the rate $\sim$3.5–5.5 W m^{-2} K^{-1} over tropical ocean descent regions, consistent with previous analysis of reanalyses and observationally derived datasets (Allan 2006). This response is dominated by enhanced cooling to the surface but is offset by increased clear-sky shortwave heating because of moistening. Increased net radiative cooling of the atmosphere is physically consistent with increases in global-mean precipitation (e.g., Allen and Ingram 2002; Held and Soden 2006; Lambert and Webb 2008).
- Models with larger Q_{LWc} response also tend to simulate a larger precipitation response to warming, although this signal is obscured for volcanically forced models.
- Over tropical oceans, simulated precipitation rises are dominated by the regions of mean ascent with increases here at the rate expected from Clausius–Clapeyron (6%–10% K^{-1}), consistent with the moisture increases that supply convective rainfall (e.g., Trenberth et al. 2003). The rate is larger for the SSM/I–HadISST datasets (18% K^{-1}); it is not clear whether this relates to the shorter time series available (1987–2000) or to differences in the microwave retrieval algorithms or to inadequacies in the models (Wentz et al. 2007; Allan and Soden 2007). Nevertheless, the lack of a signal over tropical ocean descent is expected since the mean precipitation response is balanced by the net radiative cooling of the atmosphere and is substantially less than Clausius–Clapeyron (e.g., Trenberth et al. 2003; Allan 2006).

The present study has dealt with the most well-understood aspect of the hydrological response to warming: that relating to changes in clear-sky longwave radiation (e.g., Allen and Ingram 2002). It is also important to quantify cloud longwave and shortwave radiative effects (e.g., Lambert and Webb 2008) although issues remain over the decadal changes in radiative fluxes relating to cloud and aerosol (Wielicki et al. 2002; Mishchenko et al. 2007; Wild et al. 2008; Bodas-Salcedo et al. 2008) and problems in climate monitoring remain with reanalyses and observational products struggling to accurately measure decadal changes in the hydrological cycle. Liepert et al. (2004) proposed that increases in solar absorption by aerosol may spin down the hydrological cycle. Conversely, a reduction in absorbing aerosols over recent decades (Wild et al. 2005) could contribute to increases in precipitation above the rate expected from changes in the clear-sky greenhouse effect Wild et al. (2008).

While the SSM/I record of CWV appears robust (Trenberth et al. 2005), there remains the possibility that inadequacies in the microwave retrieval algorithms

may become apparent as the climate signal emerges from natural variability. For example, the larger SSM/I precipitation sensitivity to T_s than other models and datasets for tropical ocean (Allan and Soden 2007) ascent merits further analysis. It is only by continually comparing models with observations and reanalysis products that knowledge of limitations in the observing system and understanding of the physical processes can advance.

Acknowledgments. Thanks to the WCRP for enabling the PCMDI model archive (www-pcmdi.llnl.gov). This research was supported by a UK NERC Advanced Fellowship (NE/C51785X/1) and National Centre for Earth Observation (NCEO). GPCP data were extracted from www.ncdc.noaa.gov and CMAP data from www.cdc.noaa.gov; SSM/I data were provided by Remote Sensing Systems. Thanks to Gary Strand for providing corrected NCAR PCM1 data.

REFERENCES

Adger, N., and Coauthors, 2007: Summary for policy makers. *Climate Change 2007: Impacts, Adaptation and Vulnerability,* M. L. Parry et al., Eds., Cambridge University Press, 7–22.

Adler, R. F., G. Gu, J.-J. Wang, G. J. Huffman, S. Curtis, and D. Bolvin, 2008: Relationships between global precipitation and surface temperature on interannual and longer timescales (1979–2006). *J. Geophys. Res.,* **113,** D22104, doi:10.1029/2008JD010536.

Allan, R. P., 2006: Variability in clear-sky longwave radiative cooling of the atmosphere. *J. Geophys. Res.,* **111,** D22105, doi:10.1029/2006JD007304.

——, 2007: Improved simulation of water vapour and clear-sky radiation using 24-hour forecasts from ERA40. *Tellus,* **59A,** 336–343.

——, and B. J. Soden, 2007: Large discrepancy between observed and simulated precipitation trends in the ascending and descending branches of the tropical circulation. *Geophys. Res. Lett.,* **34,** L18705, doi:10.1029/2007GL031460.

——, M. A. Ringer, and A. Slingo, 2003: Evaluation of moisture in the Hadley Centre climate model using simulations of HIRS water-vapour channel radiances. *Quart. J. Roy. Meteor. Soc.,* **129,** 3371–3389.

Allen, M. R., and W. J. Ingram, 2002: Constraints on future changes in climate and the hydrologic cycle. *Nature,* **419,** 224–232.

Bodas-Salcedo, A., M. A. Ringer, and A. Jones, 2008: Evaluation of the surface radiation budget in the atmospheric component of the Hadley Centre Global Environmental Model (HadGEM1). *J. Climate,* **21,** 4723–4748.

Chou, C., J. Tu, and P. Tan, 2007: Asymmetry of tropical precipitation change under global warming. *Geophys. Res. Lett.,* **34,** L17708, doi:10.1029/2007GL030327.

Collins, W. D., and Coauthors, 2006: The Community Climate System Model version 3 (CCSM3). *J. Climate,* **19,** 2122–2143.

Delworth, T. L., and Coauthors, 2006: GFDL's CM2 global coupled climate models. Part I: Formulation and simulation characteristics. *J. Climate,* **19,** 643–674.

Emori, S., and S. J. Brown, 2005: Dynamic and thermodynamic changes in mean and extreme precipitation under changed climate. *Geophys. Res. Lett.,* **32,** L17706, doi:10.1029/2005GL023272.

Gordon, C., C. Cooper, C. A. Senior, H. Banks, J. M. Gregory, T. C. Johns, J. F. B. Mitchell, and R. A. Wood, 2000: The simulation of SST, sea ice extents and ocean heat transports in a version of the Hadley Centre coupled model without flux adjustments. *Climate Dyn.,* **16,** 147–168.

Gordon, H. B., and Coauthors, 2002: The CSIRO Mk3 climate system model. Tech. Rep. 60, CSIRO Atmospheric Research, Aspendale, Victoria, Australia, 134 pp.

Gregory, J., and M. Webb, 2008: Tropospheric adjustment induces a cloud component in CO_2 forcing. *J. Climate,* **21,** 58–71.

Gu, G., R. F. Adler, G. J. Huffman, and S. Curtis, 2007: Tropical rainfall variability on interannual-to-interdecadal and longer time scales derived from the GPCP monthly product. *J. Climate,* **20,** 4033–4046.

Harries, J. E., and J. M. Futyan, 2006: On the stability of the Earth's radiative energy balance: Response to the Mt. Pinatubo eruption. *Geophys. Res. Lett.,* **33,** L23814, doi:10.1029/2006GL027457.

Hasumi, H., and S. Emori, 2004: K-1 coupled model (MIROC) description. K-1 Tech. Rep. 1, Center for Climate System Research, University of Tokyo, 34 pp.

Held, I. M., and B. J. Soden, 2006: Robust responses of the hydrological cycle to global warming. *J. Climate,* **19,** 5686–5699.

John, V. O., and B. J. Soden, 2007: Temperature and humidity biases in global climate models and their impact on climate feedbacks. *Geophys. Res. Lett.,* **34,** L18704, doi:10.1029/2007GL030429.

Johns, T. C., and Coauthors, 2006: The new Hadley Centre Climate Model (HadGEM1): Evaluation of coupled simulations. *J. Climate,* **19,** 1327–1353.

Jungclaus, J. H., and Coauthors, 2006: Ocean circulation and tropical variability in the coupled model ECHAM5/MPI-OM. *J. Climate,* **19,** 3952–3972.

Kalnay, E., and Coauthors, 1996: The NCEP/NCAR 40-Year Reanalysis Project. *Bull. Amer. Meteor. Soc.,* **77,** 437–471.

Kim, S. J., G. M. Flato, G. L. de Boer, and N. A. McFarlane, 2002: A coupled climate model simulation of the Last Glacial Maximum. Part I: Transient multi-decadal response. *Climate Dyn.,* **19,** 515–537.

Lambert, H. F., and M. J. Webb, 2008: Dependency of global mean precipitation on surface temperature. *Geophys. Res. Lett.,* **35,** L16706, doi:10.1029/2008GL034838.

Liepert, B., J. Feichter, U. Lohmann, and E. Roeckner, 2004: Can aerosols spin down the hydrological cycle in a moister and warmer world? *Geophys. Res. Lett.,* **31,** L06207, doi:10.1029/2003GL019060.

Marti, O., and Coauthors, 2005: The new IPSL climate system model: IPSL-CM4. Tech. Rep., Institut Pierre Simon Laplace des Sciences de l'Environment Global, Case 101, Paris, France, 84 pp.

Meehl, G. A., C. Covey, T. Delworth, M. Latif, B. McAvaneye, J. F. B. Mitchell, R. J. Stouffer, and K. E. Taylor, 2007: The WCRP CMIP3 multimodel dataset: A new era in climate change research. *Bull. Amer. Meteor. Soc.,* **88,** 1383–1394.

Mishchenko, M. I., I. V. Geogdzhayev, W. B. Rossow, B. Cairns, B. E. Carlson, A. A. Lacis, L. Liu, and L. D. Travis, 2007: Long-term satellite record reveals likely recent aerosol trend. *Science,* **315,** 1543.

Neelin, J. D., M. Munnich, H. Su, J. E. Meyerson, and C. E. Holloway, 2006: Tropical drying trends in global warming

models and observations. *Proc. Natl. Acad. Sci. USA,* **103,** 6110–6115.

Prata, A. J., 1996: A new longwave formula for estimating downwelling clear sky radiation at the surface. *Quart. J. Roy. Meteor. Soc.,* **122,** 1127–1151.

Quartly, G. D., E. A. Kyte, M. A. Srokosz, and M. N. Tsimplis, 2007: An intercomparison of global oceanic precipitation climatologies. *J. Geophys. Res.,* **112,** D10121, doi:10.1029/2006JD007810.

Rayner, N. A., D. Parker, E. Horton, C. Folland, L. Alexander, D. Rowell, E. Kent, and A. Kaplan, 2003: Global analysis of SST, sea ice and night marine air temperature since the late nineteenth century. *J. Geophys. Res.,* **108,** 4407, doi:10.1029/2002JD002670.

Richter, I., and S. P. Xie, 2008: The muted precipitation increase in global warming simulations: A surface evaporation perspective. *J. Geophys. Res.,* **113,** D24118, doi:10.1029/2008JD010561.

Salas-Mélia, D., and Coauthors, 2005: Description and validation of the CNRM-CM3 global coupled model. CNRM Working Note 103, 36 pp. [Available from Météo-France, 42 Avenue Gaspard Coriolis, 31057 Toulouse CEDEX, France.]

Schmidt, G. A., and Coauthors, 2006: Present-day atmospheric simulations using GISS ModelE: Comparison to in situ, satellite, and reanalysis data. *J. Climate,* **19,** 153–192.

Seager, R., and Coauthors, 2007: Model projections of an imminent transition to a more arid climate in southwestern North America. *Science,* **316,** 1181–1184.

Shell, K. M., J. T. Kiehl, and C. A. Shields, 2008: Using the radiative kernel technique to calculate climate feedbacks in NCAR's Community Atmospheric Model. *J. Climate,* **21,** 2269–2282.

Slingo, A., J. A. Pamment, R. P. Allan, and P. Wilson, 2000: Water vapor feedbacks in the ECMWF reanalyses and Hadley Centre climate model. *J. Climate,* **13,** 3080–3098.

Soden, B. J., D. L. Jackson, V. Ramaswamy, M. D. Schwarzkopf, and X. Huang, 2005: The radiative signature of upper tropospheric moistening. *Science,* **310,** 841–844.

Sohn, B.-J., and R. Bennartz, 2008: Contribution of water vapor to observational estimates of longwave cloud radiative forcing. *J. Geophys. Res.,* **113,** D20107, doi:10.1029/2008JD010053.

Trenberth, K. E., 2002: Changes in tropical clouds and radiation. *Science,* **296,** 2095.

——, A. Dai, R. M. Rasmussen, and D. B. Parsons, 2003: The changing character of precipitation. *Bull. Amer. Meteor. Soc.,* **84,** 1205–1217.

——, J. Fasullo, and L. Smith, 2005: Trends and variability in column-integrated atmospheric water vapor. *Climate Dyn.,* **24,** 741–758.

Uppala, S. M., and Coauthors, 2005: The ERA-40 Re-Analysis. *Quart. J. Roy. Meteor. Soc.,* **131,** 2961–3012.

Volodin, E. M., and N. A. Diansky, 2004: El Niño reproduction in coupled general circulation model. *Russ. Meteor. Hydrol.,* **12,** 5–14.

Washington, W. M., and Coauthors, 2000: Parallel climate model (PCM) control and transient simulations. *Climate Dyn.,* **16,** 755–774.

Wentz, F. J., and E. A. Francis, 1992: Nimbus-7 SMMR ocean products, 1979–1984. Remote Sensing Systems Tech. Rep. 033192, 36 pp. [Available from Remote Sensing Systems, 1101 College Ave., Santa Rosa, CA 95404.]

——, L. Ricciardulli, K. Hilburn, and C. Mears, 2007: How much more rain will global warming bring? *Science,* **317,** 233–235.

Wielicki, B. A., and Coauthors, 2002: Evidence for large decadal variability in the tropical mean radiative energy budget. *Science,* **295,** 841–844.

Wild, M., 2008: Shortwave and longwave surface radiation budgets in GCMs: A review based on the IPCC-AR4/CMIP3 models. *Tellus,* **60A,** 932–945.

——, and Coauthors, 2005: From dimming to brightening: Decadal changes in solar radiation at earth's surface. *Science,* **308,** 847–850.

——, J. Grieser, and C. Schär, 2008: Combined surface solar brightening and increasing greenhouse effect favour recent intensification of the hydrological cycle. *Geophys. Res. Lett.,* **35,** L17706, doi:10.1029/2008GL034842.

Willett, K. M., P. D. Jones, N. P. Gillett, and P. W. Thorne, 2008: Recent changes in surface humidity: Development of the HadCRUH dataset. *J. Climate,* **21,** 5364–5383.

Xie, P., and P. A. Arkin, 1998: Global monthly precipitation estimates from satellite-observed outgoing longwave radiation. *J. Climate,* **11,** 137–164.

Yang, F., A. Kumar, M. E. Schlesinger, and W. Wang, 2003: Intensity of hydrological cycles in warmer climates. *J. Climate,* **16,** 2419–2423.

Yang, H., and K. K. Tung, 1998: Water vapor, surface temperature, and the greenhouse effect—A statistical analysis of tropical-mean data. *J. Climate,* **11,** 2686–2697.

Yin, X., A. Gruber, and P. Arkin, 2004: Comparison of the GPCP and CMAP merged gauge–satellite monthly precipitation products for the period 1979–2001. *J. Hydrometeor.,* **5,** 1207–1222.

Yu, L., 2007: Global variations in oceanic evaporation (1958–2005): The role of the changing wind speed. *J. Climate,* **20,** 5376–5390.

——, and R. A. Weller, 2007: Objectively analyzed air–sea heat fluxes for the global ice-free oceans (1981–2005). *Bull. Amer. Meteor. Soc.,* **88,** 527–539.

Yukimoto, S., and A. Noda, 2002: Improvements in the Meteorological Research Institute Global Ocean-Atmosphere Coupled GCM (MRI-CGCM2) and its climate sensitivity. Tech. Rep. 10, NIES, Japan, 8 pp.

Zhang, X., F. W. Zwiers, G. C. Hegerl, F. H. Lambert, N. P. Gillett, S. Solomon, P. A. Stott, and T. Nozawa, 2007: Detection of human influence on twentieth-century precipitation trends. *Nature,* **448,** 461–465.